

Electrochemical Photocatalytic Degradation of Eriochrome Black T Dye Using Synthesized TiO₂@CNTs Nanofibers

Junren Zhu^{1,*}, Zhenzhen Jiang²

¹Chongqing City Management College, Chongqing 401331, P.R. China.

²Chongqing Vocational Institute of Engineering, Chongqing402260, P.R. China.

*E-mail: zhujunren008@163.com

Received: 18 November 2020 / Accepted: 7 January 2021 / Published: 31 January 2021

In this study, TiO₂ and TiO₂@CNTs nanofibers were synthesized via electrospinning method and their morphological, structural, optical, electrochemical properties were considered. Furthermore, these electrodes were characterized as photocatalysts for degradation of Eriochrome Black T (EBT). The network rod structure of the porous electrospun TiO₂ and TiO₂@CNTs nanofibers were observed. The high porous and large interfacial area of nanofiber of TiO₂@CNTs contained the uniform distribution and direct growth of TiO₂ on the entangled bundles carboxylate MWCNT fibers surface. Optical study showed that the optical band gap values 3.19 eV and 2.42 eV were obtained for TiO₂ and TiO₂@CNTs nanofibers, respectively which indicate preparing the hybrid system of homogeneous mixture of MWCNTs with TiO₂ narrow the band gap and develops the visible light absorption. EIS result shows that the resistance for transfer of photo-generated electrons TiO₂@CNTs nanofibers samples were lower than TiO₂. The high degradation efficiency of EBT on TiO₂@CNTs nanofibers surface was obtained under visible irradiation because of the presence of MWCNTs which lead to narrow the band gap of hybrid system and promote the effective surface area and enhance the adsorption capacity of EBT on TiO₂@CNTs nanofibers photo-catalyst surface. Moreover, recombination of photo-generated electron-hole pairs can be decreased in TiO₂@CNTs.

Keywords: Photocatalyst; Degradation efficiency; Eriochrome Black T; TiO₂@CNTs nanofibers; Photo-generated electron

1. INTRODUCTION

Nowadays, industrialization is inevitable for high demand systems and environmental contaminants and present harmful chemicals in soil, air and water are unavoidable [1, 2]. Therefore, many studies have been carried out for identification, measurement and removal of the chemicals pollution in the environment [3, 4]. Water pollution is a great concern for governments and scientists due to global warming and its consequences significantly increasing for global demand of drinking

water [5, 6]. Moreover, purgation of industrial wastewater is an effective option for water application in agriculture and other industries [7, 8].

For several decades, many investigations have been focused on organic dyes and pigments and their degradation of wastewater because of the large-scale production and outstanding applications in textiles, leather, paper printing, paint, color photography, plastics, food, pharmaceutical and cosmetics industries [9, 10]. Studies showed that many techniques such as coagulation, ultrafiltration, ozonation electrocoagulation, electroflotation, electrolysis, electrochemical oxidation and reduction, and photocatalysts have been effective techniques to remove the dye pollution from wastewaters [11, 12].

Among the different techniques for purgation of dye polluted water, photocatalytic degradation method through nanostructured semiconductors is an effective approach to remove of organic dye from aqueous solution using UV or sun lights because of its high efficiency, low cost and low energy consumption [13, 14]. Under irradiation the photons, if photons provide the required energy for excitation the electron of conduction band of semiconductors, excitation on semiconductor band gap lead to creation of electron-hole pairs. The photo-induced charges can generate radicals for degradation of the chemical dye [15].

Between the semiconductors, TiO_2 as a photocatalyst shows very remarkable properties such as environmentally friendly, high chemical and mechanical stability, low cost and low photo-corrosion[16]. Moreover, the wide band gap of TiO_2 (3.2 eV) limits its photoactivation in the UV region. In addition, the high recombination rate of photoexcited electron-hole is another important factor to limitation of TiO_2 photocatalytic activity[17, 18]. Accordingly, doping and preparing the hydride or nanocomposite of TiO_2 through the band gap engineering or architecture of the surface could improve the photodegradation efficiency. For example, Li et al. [19] applied N-doped TiO_2 for remove of dye methylene orange and presented that the removal rate of N-doped TiO_2 is significantly more than undoped TiO_2 under visible light which attributing to narrowing the band gap of N-doped TiO_2 due to N doping. Hao et al. [20] Synthesized the $\text{TiO}_2@g\text{-C}_3\text{N}_4$ core-shell photocatalysts and used them to degrade the Rhodamine B from wastewater. They showed degradation efficiency of prepared composite enhanced under the 100 Xe lamp due to formation of the band arrangement and electron migration mechanism in hybrid systems of semiconductors which impressively reduces recombination of photogenerated electrons and holes. However, the use of metal-oxide semiconductor nanostructures for the photocatalytic degradation of dyes have many advantages, no study has been conducted on the photocatalytic and electrochemical performance of $\text{TiO}_2@\text{CNTs}$ nanofibers. Therefore, in this study, TiO_2 and $\text{TiO}_2@\text{CNTs}$ nanofibers were synthesized via electrospinning method and applied as photocatalyst to photodegradation of EBT.

2. EXPERIMENT

2.1. Synthesize of $\text{TiO}_2@\text{CNTs}$ nanofibers

The electrospinning method was applied for synthesis of TiO_2 and $\text{TiO}_2@\text{CNTs}$ nanofibers through the following steps [21]. In order to promotion the chemical stability and compatibility of

CNTs on surface of TiO₂ particles, multiwall carbon nanotubes (>91%, length of 1-2 μm, diameter of 10-30nm Guangzhou Hongwu Material Technology Co., Ltd., China) were carboxylated in mixture of nitric acid (98%, Hebei Baoyi Yuequan Imp&Exp Co., Ltd., China) and sulfuric acid (98%, Langfang Jinhai Chemicals Industry Co., Ltd., China) in volume ratio 1:1 for 30 minutes. The carboxylated CNTs were washed ultrasonically with deionized water and ethanol (Shandong Sunway Chemical Co., Ltd., China) for four times, respectively and then dispersed ultrasonically in spinning solution for 120 minutes which prepared of stirred mixture of 20 ml ethanol, 2 g polyvinylpyrrolidone (PVP, average molecular weight 3.6×10^5 , Sigma-Aldrich), 2 g acetylacetone (Shandong Baovi Energy Technology Co., Ltd., China) and 10 g titanium butoxide (97%, Sigma-Aldrich). The weight ratio of CNTs to titanium butoxide were 0:1, 1:2, 1:3 and 1:4, 1:3, 1:2 and 0:1 that signified to TiO₂@CNTs, TiO₂@CNTs (1:3 w:w), TiO₂@CNTs (1:2 w:w) and TiO₂ nanofibers, respectively. The prepared mixture was transferred to a 10 ml plastic syringe which was placed on top of a stainless steel nozzle (22 gauge, length of 1 cm, inner diameter of 1 mm). Electrospinning process was conducted on NEU01 electrospinning system (5 kV, NaBond Technologies Co., Limited, Shenzhen, China) on collectors surface which contained aluminum foil or fluorine-doped tin oxide glass (FTO, Solaronix, Switzerland). The distance between the stainless-steel needle and collector was maintained at 15 cm and flow rate was adjusted 1 ml/hour. After electrospinning process, for evaporation of remaining solvents and better nucleation of TiO₂ on carboxylated CNTs surfaces, the electrospun TiO₂@CNTs nanofibers were transferred to oven and dried at 250 °C for 12 hours.

2.2. Characterization techniques

The morphology of prepared TiO₂ and TiO₂@CNTs nanofibers was analyzed by scanning electron microscopy (SEM, Zeiss supra 40vp). X-ray diffraction (XRD, D/MAX-2000, Rigaku Corporation, Tokyo, Japan) was applied to study the crystal structures of prepared samples that it conducted at power of 40 kV and 25 mA in wavelength of CuKα ($\lambda=1.5418 \text{ \AA}$). The optical absorption spectra of samples were recorded in UV-VIS spectrophotometer (TU-1901, Persee, China). EIS measurements were performed in frequency range from 10^{-3} to 10^5 Hz at a potentiostatic signal amplitude of 5 mV using potentiostat equipment (Model 263A, EG&G Instruments, Champaign, IL, USA) in a standard three-electrode electrochemical cell which containing Ag/AgCl, Pt the prepared sample as the reference electrode, counter and working electrodes, respectively. 0.1 M Na₂SO₄ (98%, Weifang Haiye Chemistry And Industry Co., Ltd., China) solution was prepared as electrolyte of EIS tests.

Photodegradation studies were carried out in a test chamber which contained a prepared samples as photocatalyst and the 100 mg/L EBT (99%, Shandong Shengpeng Sodium Silicate Co., Ltd., China) solution. UV lamps (365 nm, 8W, Philips) and visible lamps (440 nm, 8W, Philips) were used as light sources. Optical absorbance spectra of samples in the test chamber were recorded by UV-Vis diffuse reflectance spectrometer (UV-2550, Shimadzu, Kyoto, Japan). Optical absorption spectra were measured after light irradiation with a spectrophotometer (UV-2100, China). The degradation

efficiency (%) was calculated through following formula with recorded the initial absorption intensity (I_0) and photodegradation absorption intensity (I) of dye [22]:

$$\text{Degradation efficiency} = \frac{I_0 - I}{I_0} \times 100 = \frac{C_0 - C}{C_0} \times 100 \quad (1)$$

Where, C_0 and C are the initial concentration and photodegradation concentration of dye solution, respectively.

3. RESULTS AND DISCUSSION

3.1. Morphological and structural characterization

SEM analysis was carried out to evaluate the morphology of electrospun TiO_2 and TiO_2 @CNTs structures. Figure 1a shows the SEM image of electrospun TiO_2 nanofibers which contain the network structure of the porous TiO_2 membrane and rod structure. The SEM image of TiO_2 @CNTs structure in Figure 1b displays the direct growth of TiO_2 on the carboxylate MWCNT fibres surface. As shown, there are entangled bundles on the carboxylated MWCNT film which could create a high porous and unique macroscopic nanofiber structure. Electrospinning process provides condition to penetration and nucleation the TiO_2 particles into carboxylate MWCNTs pores and surface, respectively. Therefore, the uniform distribution of TiO_2 particles is formed on prepared bundles of carboxylate MWCNT fibers which lead to formation of large interfacial areas.

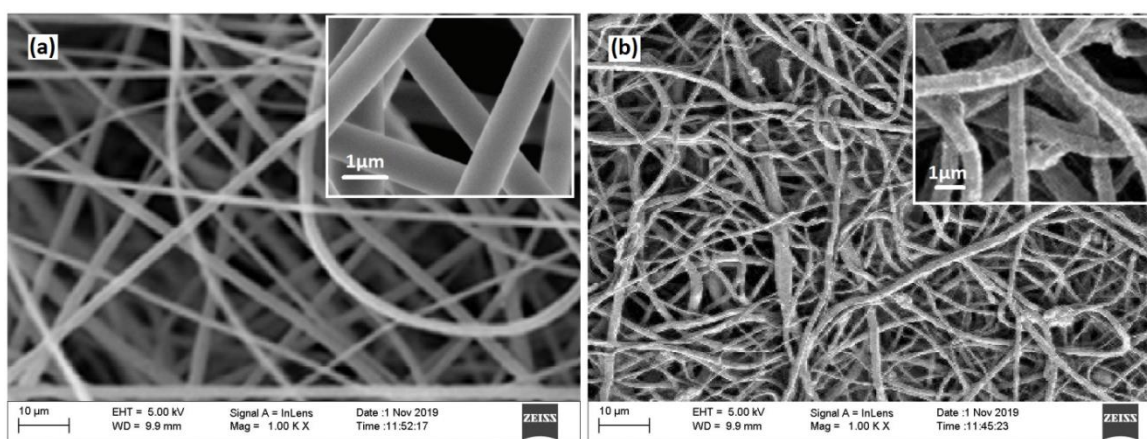


Figure 1. SEM images of (a) the electrospun TiO_2 and (b) TiO_2 @CNTs nanofibers.

In order to study the structure and crystallinity of carboxylate MWCNTs, electrospun TiO_2 and TiO_2 @CNTs nanofibers, XRD patterns of prepared samples were recorded. The XRD patterns of the carboxylate MWCNTs shows two peaks at $2\theta = 26.16^\circ$ and 44.33° which indicating to the interlayer spacing of the MWCNTs and its hexagonal graphite structure with the (002) and (100) plane, respectively [23]. The XRD patterns of the TiO_2 nanofibers exhibits the peaks at $2\theta = 25.61^\circ$, 37.79° , 48.12° , 54.04° , and 62.91° which assigning to the body-centered tetragonal TiO_2 with crystal planes of

the (101), (004), (200), (105), and (204), respectively that it is good agreement with *standard JCPDS card No. 89-4921*. The XRD patterns of the electrospun TiO₂@CNTs nanofibers shows the mixture peaks of both of carboxylated MWCNT and electrospun TiO₂ structures which implying the good match of TiO₂ on CNTs structure because of adding the carboxyl group–COOH. This group can form more active sites for interaction with TiO₂ on side walls and terminations of the MWCNTs [24, 25].

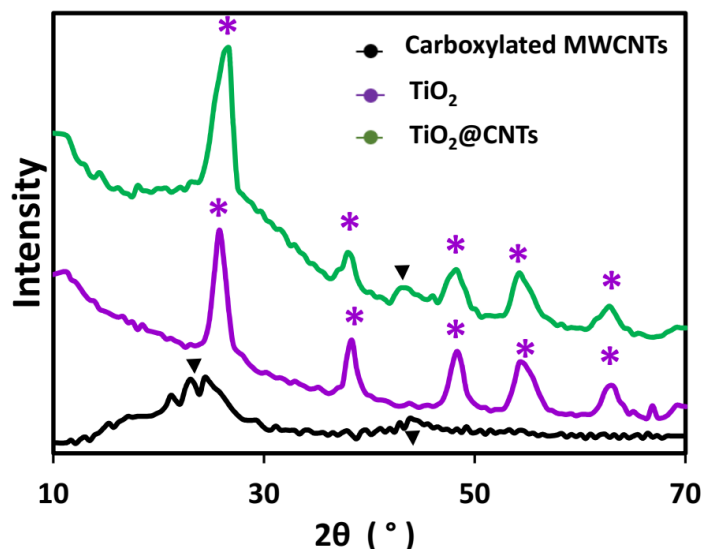


Figure 2. XRD patterns of the carboxylate MWCNTs, electrospun TiO₂ and TiO₂@CNTs nanofibers.

3.2. Optical properties

For studying the optical properties of electrospun TiO₂ and TiO₂@CNTs nanofibers, the UV-Vis absorption spectra responses of the prepared nanofibers were recorded in wavelengths ranging from 250 To 900 nm. Figure 3a shows the optical absorption spectra which illustrate a stronger visible light absorption of TiO₂@CNTs nanofibers than TiO₂ nanofibers. As shown, there is a red shift for the absorption edge of TiO₂@CNTs nanofibers that it refers to the photo-activation ability of the TiO₂@CNTs structure under irradiation of visible light range wavelength. Furthermore, it might point to the mesoporous surface of the TiO₂@CNTs nanostructure. Figure 3b displays the plot of $(\alpha h\nu)^{1/2}$ versus photon energy ($h\nu$) for determination of the optical band gap energies in prepared nanofibers where α , h and ν are absorption coefficient, Planck's constant and frequency of light, respectively. As observed, the optical band gap values 3.19 eV and 2.42 eV are obtained for TiO₂ and TiO₂@CNTs nanofibers, respectively which are very close to the reported optical band gap value by Zhou et al. [26] (3.21 eV) for TiO₂ and Darvish et al. [27] (2.87 eV) for MWCNT/TiO₂. Optical band gap of TiO₂ provides only photoactive response to ultraviolet light and only accounts for 4-5% of solar light [27]. Therefore, preparing the hybrid system of homogeneous mixture of MWCNTs with TiO₂ not only narrows the band gap and develops the visible light absorption but also leads to red shift of absorption edge of the wavelength due to chemical bonding between TiO₂ and carbon. Therefore, preparation of TiO₂@CNTs nanofibers improves the photocatalytic performance of TiO₂ in visible light.

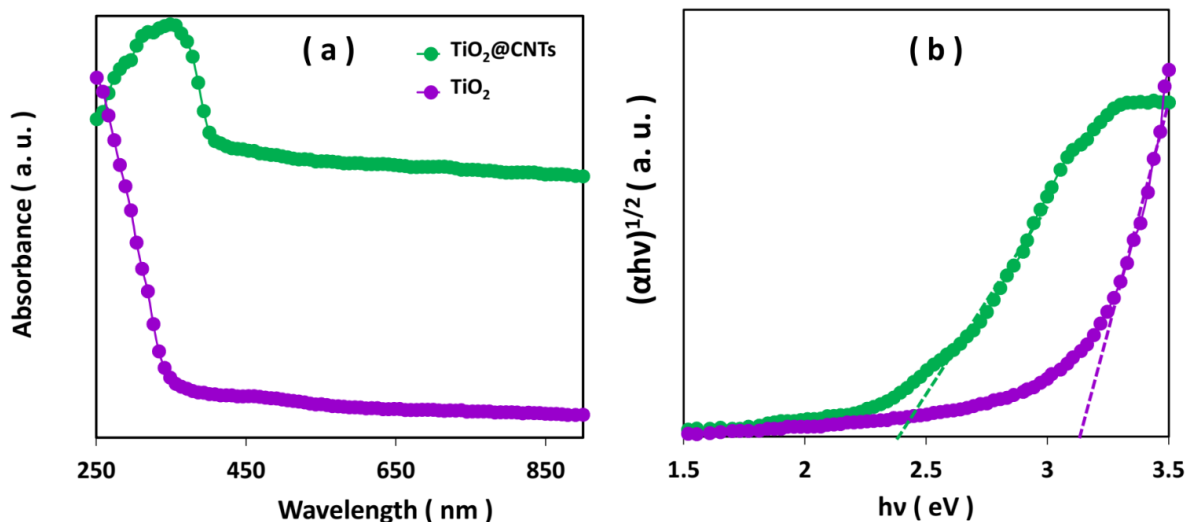


Figure 3. (a) UV-Vis absorption spectra of electrospun TiO₂ and TiO₂@CNTs nanofibers and (b) Tauc plots to determination of optical and gap values of electrospun TiO₂ and TiO₂@CNTs nanofibers.

3.4. Electrochemical impedance spectroscopy

EIS analysis was conducted for evaluating the resistance of photogenerated carriers transferring in TiO₂ and TiO₂@CNTs nanofibers [28]. The semicircle diameter of TiO₂ is more than TiO₂@CNTs nanofibers in EIS plots of Figure 4 which indicate the resistance for transfer of photogenerated electrons TiO₂@CNTs nanofibers samples is lower than TiO₂ [29, 30]. It confirms that the MWCNTs act as bridges to facilitate the electron transfer, and as consequence the photochemical quantum efficiency of TiO₂@CNTs is improved [31].

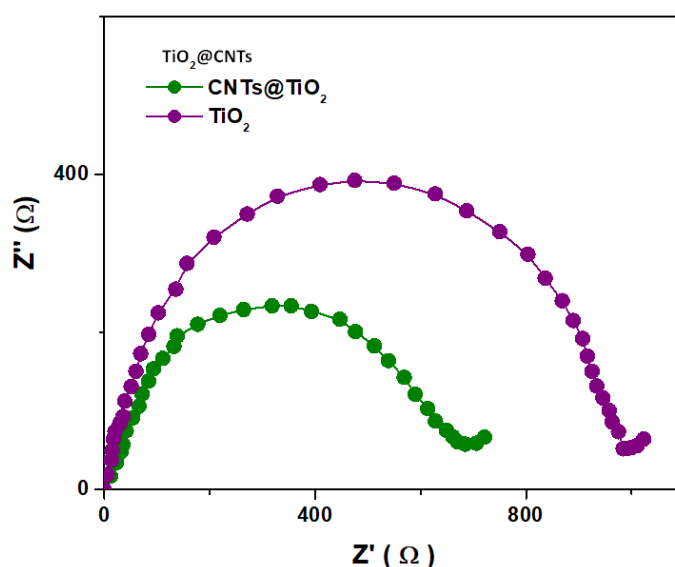


Figure 4. EIS of electrospun TiO₂ and TiO₂@CNTs nanofibers in frequency range from 10⁻³ to 10⁵ Hz at a potentiostatic signal amplitude of 5 mV in 0.1 M Na₂SO₄ as electrolyte.

3.4. Photocatalytic activity

Figure 5 displays the photocatalytic degradation of the EBT aqueous solution in darkness. As observed, the concentration of the EBT slightly decreased to 99.9%, 98.6% and 97.8% for blank samples (without catalyst), TiO_2 and TiO_2 @CNTs nanofibers, respectively under darkness condition for 5 minutes. As observed, the degradation of dye for blank samples, TiO_2 and TiO_2 @CNTs nanofibers reached to 99.8%, 97.7% and 97.1%, respectively after 30 minutes and showed relatively stable treatment for 60 minutes. In accordance with less than 1% degradation from 5 to 30 minutes, 30 minutes was considered as adsorption equilibrium time. Moreover, prior to the study of photocatalytic activity, for elimination of any light effect on measurements of photodegradation of EBT, all prepared solutions and photocatalysts were maintained in darkness for 30 minutes to reach the adsorption equilibrium.

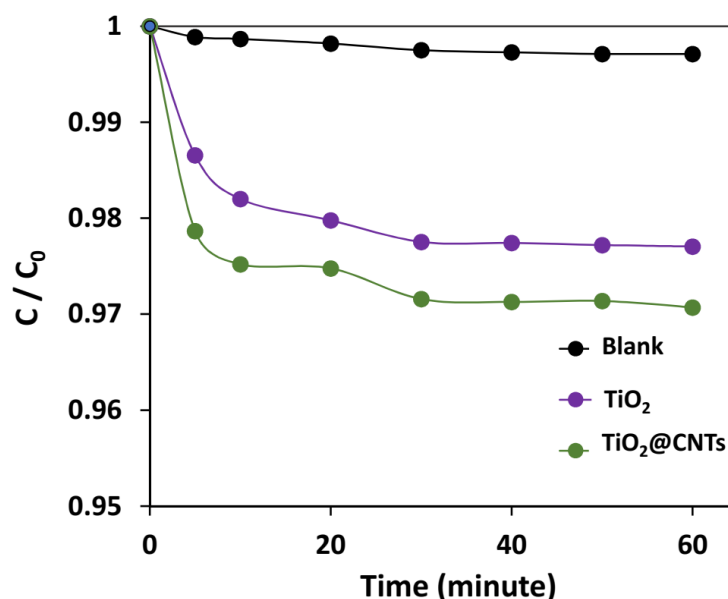


Figure 5. Photocatalytic degradation of 100 mg/L EBT in darkness for blank samples, TiO_2 and TiO_2 @CNTs nanofibers.

Figure 6 displays the photocatalytic degradation of the EBT aqueous solution under UV irradiation. As shown, degradation of EBT is increased with increasing the irradiation time of UV light for both of photocatalyst. The degradation efficiency $((C-C_0) \times 100 / C_0)$ of EBT obtained 7%, 77% and 88% for blank samples, TiO_2 and TiO_2 @CNTs nanofibers after 100 minutes UV irradiation, respectively. The results exhibits that the presence of MWCNTs increased the adsorption ability of TiO_2 nanofibers because of enhancement of the effective surface area and increase the adsorption capacity of EBT on TiO_2 @CNTs nanofibers photocatalyst surface[32]. High effective surface area and great interfacial area of prepared 1D nanostructures not only can enhance the more photoactive and sensitive sites for systems but also facilitate electron transfer through change in the electronic band structure and potential barrier [33-36]. The presence of MWCNTs can also improves the lifetime

of the photogenerated electron-hole pairs in semiconductor band gap which attributing to the difference of energy level and conduction band position between MWCNTs (4.7 eV) and TiO₂ (4.2 eV) [37, 38]. Thus, electrons in conduction band of MWCNTs are injected by TiO₂ particles and photo-excited electrons in conduction band TiO₂ can transfer to CNTs [39]. Therefore, recombination of photogenerated electron-hole pairs can be decreased in TiO₂@CNTs. Moreover, with increasing the time of UV irradiation more than 60 minutes, the degradation rate of EBT slightly decreases for both of photocatalyst [40].

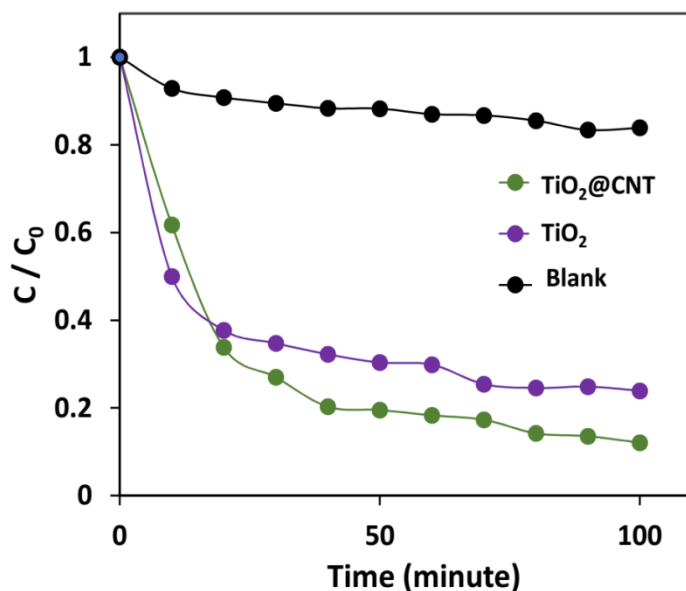


Figure 6. Photocatalytic degradation of the 100 mg/LEBT under UV irradiation for blank samples, TiO₂ and TiO₂@CNTs nanofibers.

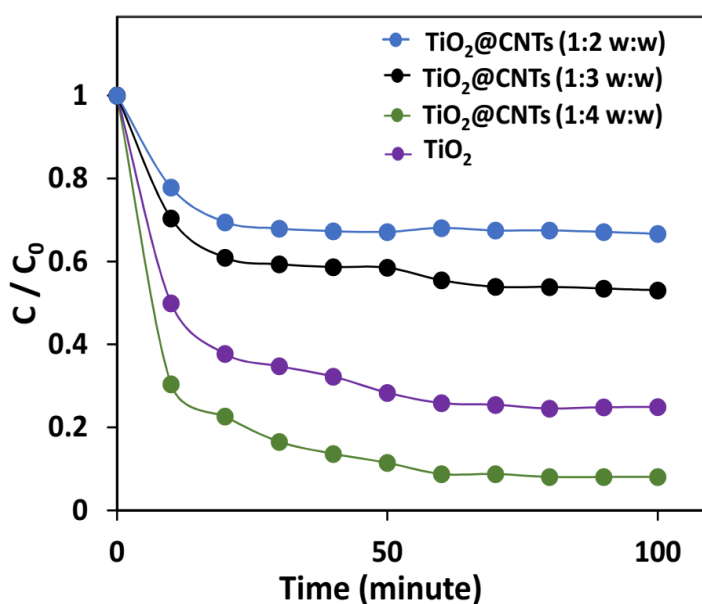


Figure 7. Photocatalytic degradation of the 100 mg/LEBT under UV irradiation for various MWCNTs concentration on TiO₂@CNTs nanofibers.

In order to study the effect of MWCNTs concentration on photocatalytic activity of TiO_2 @CNTs nanofibers, the photocatalytic degradation of EBT was also recorded on TiO_2 @CNTs (1:2 w:w) and TiO_2 @CNTs (1:3 w:w) nanofibers under UV irradiation. As observed from Figure 7, the degradation of EBT is decreased with increasing the amount of CNTs in TiO_2 @CNTs (1:3 w:w) and TiO_2 @CNTs (1:2 w:w) samples. In high concentration of MWCNTs, the addition MWCNTs completely cover TiO_2 nanofibers surface which prevents UV light from reaching the UV light and consequently it decreases the photoactivity of the resulting hybrid [41]. Therefore, the following photoactivity studies were conducted on TiO_2 @CNTs nanofibers which prepared a weight ratio of 1:4 from CNTs and TiO_2 , respectively.

For determination of the dominant species in photocatalytic reaction on TiO_2 @CNTs nanofibers surface under visible irradiation, scavenger effects measurements were recorded in present of isopropanol (IPA), triethanolamine (TEOA), Benzoquinone (BQ) and AgNO_3 as capture agents of hydroxyl radical (OH^\bullet), hole (h^+), superoxide anion radical ($\text{O}_2^{\bullet-}$) and electron (e^-), respectively [42]. Figure 8 shows decline in degradation rates of EBT after addition of IPA, TEOA, BQ and AgNO_3 . As observed, photodegradation of EBT was considerably suppressed with addition of TEOA and BQ which indicating the major effect of h^+ and $\text{O}_2^{\bullet-}$ in photodegradation of EBT on TiO_2 @CNTs nanofibers surface.

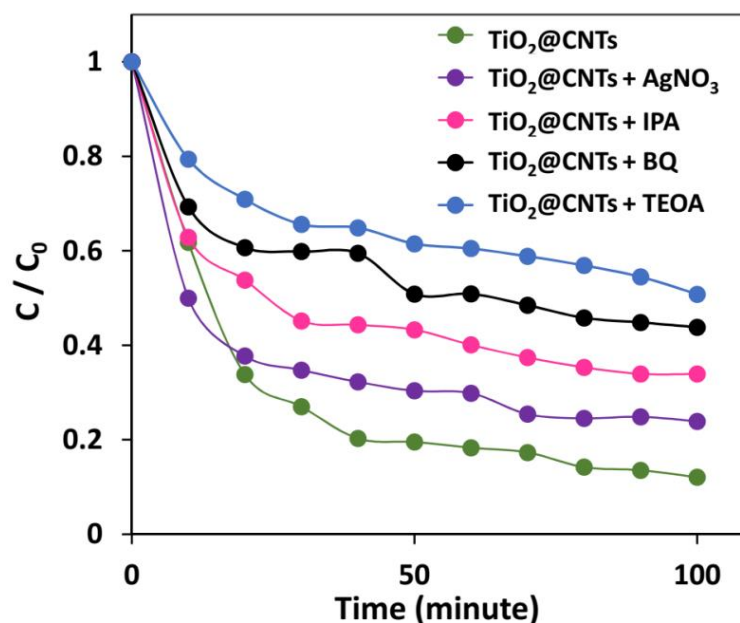


Figure 8. Photocatalytic degradation of the 100 mg/LEBT on TiO_2 @CNTs nanofibers surface under UV irradiation in present of 0.1 mg/L of IPA, TEOA, BQ and AgNO_3 .

Figure 9 shows degradation of EBT aqueous solution on prepared photocatalyst in dark and under visible and UV irradiations. The degradation efficiency of EBT obtained 15%, 88% and 92% TiO_2 @CNTs nanofibers after 100 minutes in dark and under visible and UV irradiations, respectively. As seen, there is maximum degradation efficiency of EBT on TiO_2 @CNTs nanofibers surface under

visible irradiation because of narrowing the band gap of the hybrid system of photocatalyst which benefits to absorb light in visible region [43]. Another considerable point in Figure 9 is the change in rate of degradation of EBT for both visible and UV irradiations. It found that more than 70% degradation was performed in the first 20 minute which implying the high degradation rate of EBT on TiO₂@CNTs nanofibers in first 20 minute and its fast response due to more active sites on high effective surface area of photocatalyst [44].

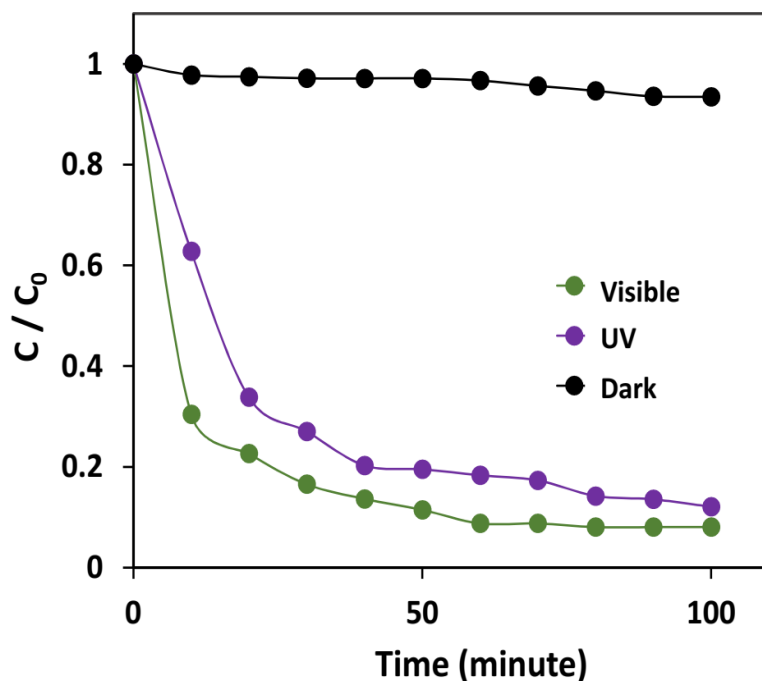


Figure 9. Photocatalytic degradation of the 100 mg/LEBT for TiO₂@CNTs nanofibers in dark and under visible and UV irradiations.

The results of this study are compared with other nanostructured materials for photodegradation efficiency of EBT. This comparison is displayed in Table 1. Comparison shows that the better photocatalytic behavior of synthesized TiO₂@CNTs which can be attributed to morphology, small particle size, high crystallinity of TiO₂@CNTs. Moreover, improvement of photocatalytic activity in TiO₂@CNTscan be related to the formation of a synergistic heterojunction, which facilitates a fast electron transfer at the interface between CNTs and TiO₂and promotes charge separation and stabilization and decreased the recombination of photo-induced electron-hole pairs in the TiO₂@CNTs composite [45, 46].The introduction of CNT into the titanium matrix induced a synergic effect when irradiating in the near-UV to visible spectral range. This effect may be explained in terms of a strong interphase interaction between CNT and TiO₂ in the composite catalysts. CNT with different surface chemical groups were used to produce TiO₂@CNTs composites [47]. Therefore, the novelty of this work lies in the use of TiO₂@CNTs as photocatalysis to degradation of the EBT under visible irradiation.

Table 1. Comparison between the results of this study with other nanostructured materials for photodegradation efficiency of EBT.

material	Dye content (mg/L)	Light source	Degradation time (minute)	Degradation efficiency (%)	ref
TiO ₂ @CNTs	100	visible	100	88	This work
TiO ₂ @CNTs	100	UV	100	92	This work
ZnO@Ag ₂ S core-shell nanoparticles	40	UV	120	69	[48]
ZnO nanoparticles	40	UV	120	37	[48]
TiO ₂ nanoparticles	25	UV	90	82	[49]
TiO ₂ (PC-50)	25	UV	90	35	[49]
TiO ₂ (PC-500)	25	UV	90	51	[49]
ZnO (Merck)	25	UV	90	62	[49]
TiO ₂ nanoparticles	100	UV	150	65	[50]
Eu-doped ZnO	100	UV	240	100	[51]
SnO ₂ -bentonite nanocomposite	100	UV	300	100	[52]

4. CONCLUSION

The electrospinning method was applied for synthesis of TiO₂ and TiO₂@CNTs nanofibers. The SEM, XRD, UV-Vis absorption spectra, EIS and photocatalytic analyses were conducted for characterization morphological, structural, optical, electrochemical and photodegradation properties of TiO₂ and TiO₂@CNTs nanofibers. The high porous and large interfacial area of TiO₂@CNTs nanofiber contained the uniform distribution and direct growth of TiO₂ on the entangled bundles carboxylate MWCNT fibers surface. Optical absorption spectra showed a stronger visible light absorption of TiO₂@CNTs nanofibers than TiO₂ nanofibers. The optical band gap values 3.19 eV and 2.42 eV were obtained for TiO₂ and TiO₂@CNTs nanofibers, respectively which indicate the homogeneous hybrid mixture of MWCNTs with TiO₂ not only narrow the band gap and develop the visible light absorption. The EIS showed the resistance for transfer of photo-generated electrons TiO₂@CNTs nanofibers samples was lower than TiO₂. Photocatalytic studies showed that the degradation efficiency of EBT obtained 77% and 88% for TiO₂ and TiO₂@CNTs nanofibers after 100 minutes UV irradiation, respectively. The high degradation efficiency of EBT on TiO₂@CNTs nanofibers surface under visible irradiation because of narrowing the band gap of the hybrid system. These results indicate that the prepared TiO₂@CNTs nanofibers improve the photocatalytic performance of TiO₂ in visible light.

ACKNOWLEDGEMENT

The authors are grateful for the financial support provided by the Scientific and Science and Technology Research Program of Chongqing Municipal Education Commission (Grant No.KJQN202003306, No.KJQN201903408 and No.KJQN201803307), and Natural Science Foundation of Chongqing (Grant No.cstc2020jcyj-msxmX0949)

References

1. T. Mahanty, S. Bhattacharjee, M. Goswami, P. Bhattacharyya, B. Das, A. Ghosh and P. Tribedi, *Environmental Science and Pollution Research*, 24(2017)3315.
2. H. Karimi-Maleh and O.A. Arotiba, *Journal of colloid and interface science*, 560(2020)208.
3. C. Teodosiu, A.-F. Gilca, G. Barjoveanu and S. Fiore, *Journal of cleaner production*, 197(2018)1210.
4. R. Dalvand, S. Mahmud, J. Rouhi and C.R. Ooi, *Materials Letters*, 146(2015)65.
5. J. Vasco-Correa, S. Khanal, A. Manandhar and A. Shah, *Bioresource technology*, 247(2018)1015.
6. H. Karimi-Maleh, Y. Orooji, A. Ayati, S. Qanbari, B. Tanhaei, F. Karimi, M. Alizadeh, J. Rouhi, L. Fu and M. Sillanpää, *Journal of Molecular Liquids*, (2020)115062.
7. H.F.B. Lasta, L. Lentz, L.G.G. Rodrigues, N. Mezzomo, L. Vitali and S.R.S. Ferreira, *Biocatalysis and Agricultural Biotechnology*, 21(2019)101353.
8. M. Miraki, H. Karimi-Maleh, M.A. Taher, S. Cheraghi, F. Karimi, S. Agarwal and V.K. Gupta, *Journal of Molecular Liquids*, 278(2019)672.
9. S. Samsami, M. Mohamadi, M.-H. Sarrafzadeh, E.R. Rene and M. Firoozbahr, *Process Safety and Environmental Protection*, 143(2020)138.
10. J. Rouhi, C.R. Ooi, S. Mahmud and M.R. Mahmood, *Electronic Materials Letters*, 11(2015)957.
11. A. Alinsafi, M. Khemis, M.-N. Pons, J.-P. Leclerc, A. Yaacoubi, A. Benhammou and A. Nejmeddine, *Chemical engineering and processing: Process intensification*, 44(2005)461.
12. H. Karimi - Maleh, F. Karimi, M. Alizadeh and A.L. Sanati, *The Chemical Record*, 20(2020)682.
13. M.S. Hussien and I. Yahia, *Journal of Photochemistry and Photobiology A: Chemistry*, 368(2019)210.
14. J. Rouhi, S. Mahmud, S. Hutagalung and S. Kakooei, *Micro & Nano Letters*, 7(2012)325.
15. L. Collado, A. Reynal, F. Fresno, M. Barawi, C. Escudero, V. Perez-Dieste, J.M. Coronado, D.P. Serrano, J.R. Durrant and A. Víctor, *Nature communications*, 9(2018)1.
16. F. Tahernejad-Javazmi, M. Shabani-Nooshabadi and H. Karimi-Maleh, *Composites Part B: Engineering*, 172(2019)666.
17. H. Karimi-Maleh, K. Cellat, K. Arıkan, A. Savk, F. Karimi and F. Şen, *Materials Chemistry and Physics*, 250(2020)123042.
18. M. Alimanesh, J. Rouhi and Z. Hassan, *Ceramics International*, 42(2016)5136.
19. H. Li, Y. Hao, H. Lu, L. Liang, Y. Wang, J. Qiu, X. Shi, Y. Wang and J. Yao, *Applied Surface Science*, 344(2015)112.
20. J. Hao, S. Zhang, F. Ren, Z. Wang, J. Lei, X. Wang, T. Cheng and L. Li, *Journal of colloid and interface science*, 508(2017)419.
21. M. Wongaree, S. Chiarakorn, S. Chuangchote and T. Sagawa, *Environmental Science and Pollution Research*, 23(2016)21395.
22. A.V. Borhade, D.R. Tope and B.K. Uphade, *E-Journal of Chemistry*, 9(2012)705.
23. Z. Abousalman-Rezvani, P. Eskandari, H. Roghani-Mamaqani and M. Salami-Kalajahi, *Advances in Colloid and Interface Science*, (2020)102126.
24. I.V. Zaporotskova, N.P. Boroznina, Y.N. Parkhomenko and L.V. Kozhitov, *Modern Electronic Materials*, 2(2016)95.
25. J. Rouhi, H.K. Malayeri, S. Kakooei, R. Karimzadeh, S. Alrokayan, H. Khan and M.R. Mahmood, *International Journal of Electrochemical Science*, 13(2018)9742.
26. Z. Zhou and H. Wang, *International Journal of Photoenergy*, 2014(2014)568185.
27. S. Mohammad Darvish, A. Mortezaali and S. RamezaniSani, *Journal of Interfaces, Thin Films and Low dimensional systems*, 2(2019)149.
28. J. Rouhi, S. Kakooei, M.C. Ismail, R. Karimzadeh and M.R. Mahmood, *International Journal*

- of Electrochemical Science*, 12(2017)9933.
29. H. Salavati, A. Teimouri and S. Kazemi, *Int J Electrochem Sci*, 13(2018)2887.
 30. H. Long, D. Tan, S. Wang, Z. Wang, Y. Deng and S. Zhang, *Int. J. Electrochem. Sci*, 15(2020)4534.
 31. L. Yang, Y. Luo, L. Yang, S. Luo, X. Luo, W. Dai, T. Li and Y. Luo, *Journal of hazardous materials*, 367(2019)550.
 32. Y. Yu, C.Y. Jimmy, C.-Y. Chan, Y.-K. Che, J.-C. Zhao, L. Ding, W.-K. Ge and P.-K. Wong, *Applied Catalysis B: Environmental*, 61(2005)1.
 33. F. Chahshouri, H. Savaloni, E. Khani and R. Savari, *Journal of Micromechanics and Microengineering*, 30(2020)075001.
 34. H. Savaloni, R. Savari and S. Abbasi, *Current Applied Physics*, 18(2018)869.
 35. R. Savari, H. Savaloni, S. Abbasi and F. Placido, *Sensors and Actuators B: Chemical*, 266(2018)620.
 36. S. Kang, L. Zhang, T. Xu, M. He, M. Chen, Q. Wang, D. Sun and X. Chang, *Int. J. Electrochem. Sci*, 13(2018)10679.
 37. O.R. Fonseca-Cervantes, A. Pérez-Larios, V.H. Romero Arellano, B. Sulbaran-Rangel and C.A. Guzmán González, *Processes*, 8(2020)1032.
 38. C. Maheu, L. Cardenas, E. Puzenat, P. Afanasiev and C. Geantet, *Physical Chemistry Chemical Physics*, 20(2018)25629.
 39. M. Shaban, A.M. Ashraf and M.R. Abukhadra, *Scientific reports*, 8(2018)1.
 40. M. Pawar, S. Topcu Sendoğdular and P. Gouma, *Journal of Nanomaterials*, 2018(2018)1.
 41. T.H.T. Vu, H.T. Au, T.T.T. Nguyen, M.H. Do, M.T. Pham, D.H. Bui, T.S. Phan and D.L. Nguyen, *Journal of Sulfur Chemistry*, 38(2017)264.
 42. Q. Li, K. Wang, X. Lu, R. Luo, M. Zhang, C. Cui and G. Zhu, *Int. J. Electrochem. Sci*, 15(2020)9256.
 43. T. Gao, G. Sun, F. Cheng, K. Dai, H. Chen, K. Deng and Q. Huang, *Rsc Advances*, 5(2015)28973.
 44. J. Ge, Y. Zhang, Y.-J. Heo and S.-J. Park, *Catalysts*, 9(2019)122.
 45. K. Sridharan, E. Jang and T.J. Park, *Applied Catalysis B: Environmental*, 142(2013)718.
 46. C.-H. Wu, C.-Y. Kuo and S.-T. Chen, *Environmental technology*, 34(2013)2513.
 47. C.G. Silva and J.L. Faria, *Applied Catalysis B: Environmental*, 101(2010)81.
 48. A. Sadollahkhani, I. Kazeminezhad, O. Nur and M. Willander, *Materials Chemistry and Physics*, 163(2015)485.
 49. S.K. Kansal, S. Sood, A. Umar and S.K. Mehta, *Journal of Alloys and Compounds*, 581(2013)392.
 50. A. Gautam, A. Kshirsagar, R. Biswas, S. Banerjee and P.K. Khanna, *RSC advances*, 6(2016)2746.
 51. P. Franco, O. Sacco, I. De Marco, D. Sannino and V. Vaiano, *TOPICS IN CATALYSIS*, 63(2020)1193.
 52. M. Honarmand, M. Golmohammadi and A. Naeimi, *Materials Chemistry and Physics*, 241(2020)122416.